*Journal of Statistical Physics, Vol. 122, No. 6, March 2006 (© 2006)*
DOI: 10.1007/s10955-006-9028-8

# Thin-Film Flow Influenced by Thermal Noise

**Günther Grün,[1] Klaus Mecke,[2] and Markus Rauscher[3]**

*Received April 14, 2005; accepted October 25, 2005*
*Published Online: March 15, 2006*

We study the influence of thermal fluctuations on the dewetting dynamics of thin liquid films. Starting from the incompressible Navier-Stokes equations with thermal noise, we derive a fourth-order degenerate parabolic stochastic partial differential equation which includes a conservative, multiplicative noise term—the stochastic thin-film equation. Technically, we rely on a long-wave-approximation and Fokker–Planck-type arguments. We formulate a discretization method and give first numerical evidence for our conjecture that thermal fluctuations are capable of accelerating film rupture and that discrepancies with respect to time-scales between physical experiments and deterministic numerical simulations can be resolved by taking noise effects into account.

**KEY WORDS:** wetting, microfluidics, thin film flow, stochastic hydrodynamics

## 1. INTRODUCTION

Thin films of liquid are ubiquitous in nature and play a great role in technological processes. Progressive miniaturization in the production of semiconductor devices requires nowadays thicknesses of photo resists of the order of a few nanometers. In order to guarantee stability of these films reliable predictions of the dynamics (in particular of the dewetting dynamics) gain an important role. But also in the emerging field of micro and nano fluidics, i.e., the art of miniaturizing chemical devices, one deals with fluid films of down to a few nanometers thickness.

[1] Institut für Angewandte Mathematik, Universität Bonn, Beringstr. 6, 53115 Bonn, Germany; e-mail: gg@iam.uni-bonn.de
[2] Institut für Theoretische Physik, Universität Erlangen-Nürnberg, Staudtstr. 7/B3, 91058 Erlangen, Germany; e-mail: klaus.mecke@physik.uni-erlangen.de
[3] Max-Planck-Institut für Metallforschung, Heisenbergstr. 3, 70569 Stuttgart, Germany, and ITAP, Universität Stuttgart, Pfaffenwaldring 57, 70569 Stuttgart, Germany; e-mail: rauscher@mf.mpg.de

The flow of viscous liquid films with thicknesses in the range of a few nanometers up to a micron has been studied extensively in the thin-film limit of hydrodynamic free surface flow.[1] While earlier studies focused on spreading of droplets and the moving three phase contact line, the dewetting of thermodynamically unstable liquid films and the resulting dewetting patterns have attracted more attention recently. In particular, the development of efficient numerical algorithms for the thin-film equation (see[2,3] and the references therein) and of quantitative methods based on integral measures (Minkowsky functionals) for describing and comparing film morphologies[4] made it possible to test the thin-film equation quantitatively. While the spatial stochastic features of the pattern formation process which appear in the experiment are the same as those predicted by the thin-film equation,[5] the time evolution of the patterns does not match. The quantities which characterize the morphology of the experimental films as a function of time indicate a power law behavior while the numerical results for the deterministic thin film equation show two distinct time scales, one for film rupture and one for droplet formation, see.[6] We take this as a hint that thermal noise might play a role in the dynamics of the dewetting of these thin films. Power law behaviour can indicate the absence of explicit time scales, which is characteristic for thermal fluctuations modeled by white noise.

The effect of thermal noise has already been introduced phenomenologically into hydrodynamics by Landau and Lifšic.[7] A microscopic justification for the noisy hydrodynamical equations has been provided by showing that the form proposed can be derived from the deterministic Boltzmann equation by a long-wave approximation.[8] The noisy hydrodynamical equations have been discussed for example in the context of turbulence in randomly stirred fluids[9,10] as well as for the onset of instabilities in Rayleigh-Bénard convection[11] and Taylor-Couette flow.[12]

Comparing molecular dynamics simulations and numerical solutions of deterministic and stochastic hydrodynamical equations[13] it has recently become evident that noise plays a significant role in the breakup of fluid nanojets. The geometry is cylindrical rather than planar but a long-wave approximation similar to the one discussed in this paper is used. This result corroborates our conjecture that thermal noise can play a significant role in the dewetting and flow of thin liquid films.

The importance of thermal fluctuations in film rupture has been demonstrated by direct visual observation in a colloidal system with confocal microscopy.[14] Suspended colloids can phase-separate into regions of high density ("colloidal liquid") and low density ("colloidal gas"). The coalescence of two drops of "colloidal liquid" involves the rupture of a thin film of "colloidal gas" which has been monitored directly. The importance of fluctuations is obvious from visual inspection but has not been quantified yet.

Let us give the outline of the paper. Starting from the incompressible Navier-Stokes equations with thermal noise, we formulate in Sec. 2.1 the free surface problem for thin-film flow under the influence of fluctuations. In Sec. 2.2, we derive a first version of a stochastic thin-film equation via long-wave approximation. It contains a rather complicated noise term which involves a stochastic integral with respect to the vertical coordinate. By requiring the corresponding Fokker–Planck equations to be identical, we come up with a simplified stochastic thin-film equation which involves a noise term only depending on planar coordinates and time. The scaling of the off-diagonal components of the noisy stress tensor is crucial for the formulation of both equations. Our choice guarantees that the invariant measure is given by the Gibbs distribution.

Section 3 is devoted to the study of effects thermal fluctuations have on dewetting dynamics. We base our results on numerical simulations and propose a finite-volume/finite-element scheme for the discretization of the stochastic thin-film equation first. Our numerical experiments give first indication that noise can accelerate the transition from a nearly flat film to a locally ruptured film. In contrast, the time-scale of droplet formation is not affected by fluctuations in these experiments. Therefore, the ratio

$$\frac{\text{rupture time-scale}}{\text{droplet-formation time-scale}}$$

is diminished. This leads us to believe, that discrepancies with respect to time-scales between deterministic numerical simulations and physical experiments observed in[5] might be overcome by taking thermal fluctuations into account. To give further evidence for this conjecture, we estimate the strength of the noise term in the experimental setting of.[5] It turns out that the acceleration factor observed in the numerical experiments presented here has the right order of magnitude to resolve the aforementioned discrepancies.

Finally, Appendix A contains the computation of the Kramers–Moyal coefficients needed in Sec. 2.2, and Appendix B reviews the numerical scheme for the deterministic thin-film equation. In Appendix C we show that the Fokker–Planck equation of the stochastic thin film quation derived in Sec. 2.2 is independent of the stochastic calculus (Ito or Stratonovich) used.

## 2. THE STOCHASTIC THIN-FILM EQUATION

### 2.1. Noise in the Hydrodynamic Equations

For the ease of presentation, we consider a film of an incompressible Newtonian liquid on a one-dimensional flat substrate as sketched in Fig. 1. The generalization to two-dimensional films is straightforward. Since we do not want

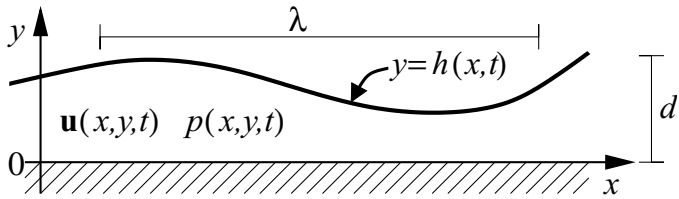


**Fig. 1.** A thin liquid film on a flat one-dimensional substrate (coinciding with the $x$-axis). The film surface (i.e., the moving boundary) is parameterized by the film thickness $h(x, t)$. The flow is characterized by the flow velocity $\mathbf{u} = (u_x, u_y)$ and the pressure $p$.

to discuss boundary conditions at the boundaries of the substrate, we suppose the substrate to be infinite. We assume that the liquid-vapour interface can be described as a graph over the substrate, and we parameterize it by the film thickness $h(x, t)$. The incompressibility condition and the momentum conservation are given by[7]

$$0 = \nabla \cdot \mathbf{u} \tag{1}$$

$$\rho \frac{\mathrm{D}\mathbf{u}}{\mathrm{D}t} = \eta \nabla^2 \mathbf{u} - \nabla p + \nabla \cdot \boldsymbol{\mathcal{S}}, \tag{2}$$

with the convective derivative $\frac{\mathrm{D}}{\mathrm{D}t} = \frac{\partial}{\partial t} + \mathbf{u} \cdot \nabla$. By $\mathbf{u}$ and $p$, we denote velocity and pressure field, respectively. The mass density $\rho$ is constant within the fluid and $\eta$ is the shear viscosity. The random stress fluctuations $\boldsymbol{\mathcal{S}}$ represent the effect of molecular motion. $\boldsymbol{\mathcal{S}}$ is symmetric, has zero mean $\langle \boldsymbol{\mathcal{S}} \rangle = 0$ and the correlator is given as

$$\left\langle \mathcal{S}_{ij}(\mathbf{r}, t)\, \mathcal{S}_{lm}(\mathbf{r}', t') \right\rangle = 2\, \eta\, k_B\, T\, \delta(\mathbf{r} - \mathbf{r}')\, \delta(t - t')\, (\delta_{il}\, \delta_{jm} + \delta_{im}\, \delta_{jl}). \tag{3}$$

$\boldsymbol{\mathcal{S}}$ is spatially uncorrelated, and therefore the divergence of $\boldsymbol{\mathcal{S}}$ in Eq. (2) poses mathematical questions we do not want to enter into at this point. From a physical point of view, hydrodynamical equations are only valid at a scale large as compared to the molecular scale. Therefore, $\delta(\mathbf{r} - \mathbf{r}')$ in Eq. (3) might be replaced by a correlation function of small but finite width. In order to show that equilibria are charcterized by Gaussian velocity distributions as required by thermodynamics we need spatially uncorrelated noise. For this reason, we keep the notation common in physical literature.

We assume that the substrate is impermeable and that there is no slip between the fluid and the substrate. The boundary conditions at the substrate are therefore

$$u_y = 0 \quad \text{and} \quad u_x = 0 \quad \text{at} \quad y = 0. \tag{4}$$

At the free surface $z = h(x, t)$ the normal and tangential stresses are balanced. Neglecting the exchanges with the vapour phase, the boundary condition is

$$(\boldsymbol{\sigma} + \boldsymbol{\mathcal{S}}) \cdot \hat{\mathbf{n}} = (\Pi + \gamma\, \kappa)\, \hat{\mathbf{n}}, \tag{5}$$

where $\sigma_{ij} = \eta\,(\partial_i u_j + \partial_j u_i) - p\,\delta_{ij}$ is the stress tensor for an incompressible fluid, $\kappa$ is the mean curvature of the surface, $\hat{\mathbf{n}} = (-\partial_x h, 1)/\sqrt{1 + (\partial_x h)^2}$ the surface normal vector, and $\gamma$ is the surface tension coefficient. For later use we also introduce the tangent vector $\hat{\mathbf{t}} = (1, \partial_x h)/\sqrt{1 + (\partial_x h)^2}$ to the surface. The so-called disjoining pressure $\Pi = -\frac{\partial \Phi(h)}{\partial h}$ is the negative derivative of the effective interface potential $\Phi(h)$ with respect to the film thickness $h$. The origin of the disjoining pressure are molecular interactions between liquid molecules and between liquid and substrate molecules. The disjoining pressure determines the characteristic wetting properties of a substrate, for instance the equilibrium contact angle. In general, the disjoining pressure can depend on $x$ and $y$. Additional external forces on the fluid such as gravity or Marangoni forces can be included in a straightforward manner.

Finally, assuming that the fluid is non-volatile, the component of the flow velocity normal to the surface is identical to the surface normal velocity and we get

$$\frac{\partial h}{\partial t} = u_y - u_x\, \partial_x h \quad \text{at} \quad y = h \tag{6a}$$

$$= -\partial_x j, \tag{6b}$$

with the total flow current in the film at position $x$

$$j(x, t) = \int_0^{h(x,t)} u_x(x, y, t)\, dy. \tag{7}$$

## 2.2. Long-Wave Approximation of Stochastic Navier-Stokes Equations

The long-wave approximation permits to approximate the free surface problem for thin films stated in Sec. 2.1 by a dimension-reduced evolution equation for the film height. The small parameter $\varepsilon = d/\lambda \ll 1$ in this approximation is the ratio of the characteristic film height $d$ and the length scale $\lambda$ over which the film thickness and substrate properties (e.g., $\Pi$) vary laterally, see Fig. 1. This approach is well described in[1] but we will recapitulate the main steps with an emphasis on the noise term $\boldsymbol{\mathcal{S}}$, which was not considered in.[1] In order to implement the long-wave expansion, we express all quantities in Eqs. (1)–(7) in terms of dimensionless quantities denoted by a tilde. Introducing a characteristic velocity $U$ in

the film parallel to the substrate, we use the rescaling relations

$$\begin{aligned}
x &= \lambda\,\tilde{x}, & y &= d\,\tilde{y}, & p &= \frac{U\,\eta}{d\,\varepsilon}\,\tilde{p},\\
\partial_x &= \frac{1}{\lambda}\,\tilde{\partial}_x, & \partial_y &= \frac{1}{d}\,\tilde{\partial}_y, & \Pi &= \frac{U\,\eta}{d\,\varepsilon}\,\tilde{\Pi},\\
u_x &= U\,\tilde{u}_x, & u_y &= \varepsilon\,U\,\tilde{u}_y, & t &= \frac{\lambda}{U}\,\tilde{t},\\
\gamma &= \frac{U\,\eta}{\varepsilon^3}\,\tilde{\gamma}, & \kappa &= \frac{\varepsilon^2}{d}\,\tilde{\kappa}, & h &= d\,\tilde{h},\\
\mathcal{S}_{xy} &= \frac{U\,\eta}{d}\,\tilde{\mathcal{S}}_{xy} & (\mathcal{S}_{xx}, \mathcal{S}_{yy}) &= \frac{U\,\eta}{\lambda}\,(\tilde{\mathcal{S}}_{xx}, \tilde{\mathcal{S}}_{yy}) & T &= \frac{\eta\,U\,\lambda^2}{\epsilon\,k_B}\,\tilde{T}.
\end{aligned} \tag{8}$$

Thereby we assume that the components of the noise tensor scale like the dominant term (lowest order in $\varepsilon$) in the corresponding components of the strain tensor. For $\mathcal{S}_{xx}$ and $\mathcal{S}_{yy}$ these are $\eta\,\partial_x u_x$ and $\eta\,\partial_y u_y$, respectively. For $\mathcal{S}_{xy}$ (which is equal to $\mathcal{S}_{yx}$ due to symmetry) this is $\eta\,\partial_y u_x$. Hence, the noise tensor will appear in the lowest order equations of motion in such a way that the stationary height distribution of the resulting thin-film Eq. (17) is the one required by thermodynamics (see Sec. 2.3). This justifies our way of rescaling retrospectively. The final result would remain unchanged if $\mathcal{S}_{xx}$ and $\mathcal{S}_{yy}$ scaled in the same way as $\mathcal{S}_{xy}$. In addition to $\varepsilon \ll 1$, lubrication approximation assumes that the flow is not too fast and that the viscosity is not too low so that the Reynolds number $\mathrm{Re} = \rho\,U\,d/\eta$ is of order one or smaller. We note that the surface tension coefficient $\gamma$ is scaled with $\varepsilon^{-3}$. This ensures that surface tension is kept in the equations to lowest order in the thin-film limit $\varepsilon \to 0$. Unless explicitly stated otherwise, all quantities are nondimensional from this point on and we therefore drop the tilde.

The incompressibility condition Eq. (1) remains unchanged under these rescalings. For the parallel and normal components of the momentum Eq. (2) we get

$$\begin{aligned}
\varepsilon\,\mathrm{Re}\,\frac{\mathrm{D}u_x}{\mathrm{D}t} &= \left(\varepsilon^2\,\partial_x^2 + \partial_y^2\right)u_x - \partial_x(p+\Pi)\\
&\quad + \varepsilon^2\,\partial_x\mathcal{S}_{xx} + \partial_y\mathcal{S}_{yx} \qquad (9a)\\
\varepsilon^3\,\mathrm{Re}\,\frac{\mathrm{D}u_y}{\mathrm{D}t} &= \varepsilon^2\left(\varepsilon^2\,\partial_x^2 + \partial_y^2\right)u_y - \partial_y(p+\Pi)\\
&\quad + \varepsilon^2\,\partial_x\mathcal{S}_{xy} + \varepsilon^2\,\partial_y\mathcal{S}_{yy}. \qquad (9b)
\end{aligned}$$

Clearly, the noise term will only appear in the equation for $u_x$, and we get the principal equations

$$0 = -\partial_x(p+\Pi) + \partial_y^2 u_x + \partial_y\mathcal{S}_{yx} \tag{10a}$$

$$0 = -\partial_y(p+\Pi). \tag{10b}$$

The boundary conditions at the substrate (4) as well as the kinematic condition (6) remain unchanged. We discuss the boundary conditions at the surface (5) in the following. The curvature is to lowest order $\kappa = \partial_x^2 h + \mathcal{O}\left(\varepsilon^4\right)$ and the normal component of the normal surface stress is $\hat{\mathbf{n}} \cdot (\boldsymbol{\sigma} + \boldsymbol{\mathcal{S}}) \cdot \hat{\mathbf{n}} = -p + \mathcal{O}\left(\varepsilon^2\right)$. Therefore we get the boundary condition for the pressure at the liquid-vapor interface

$$p = -\gamma\, \partial_x^2 h \quad \text{at} \quad y = h. \tag{11}$$

The tangential component of the normal surface stress is

$$\hat{\mathbf{t}} \cdot (\boldsymbol{\sigma} + \boldsymbol{\mathcal{S}}) \cdot \hat{\mathbf{n}} = \frac{(\partial_x h)\,(\partial_y u_x + \mathcal{S}_{yx})}{|\partial_x h|} + \mathcal{O}\left(\varepsilon^2\right) \quad \text{at} \quad y = h \tag{12}$$

and we obtain the following boundary condition for $u_x$ at the film surface

$$\partial_y u_x + \mathcal{S}_{yx} = 0 \quad \text{at} \quad y = h. \tag{13}$$

Apparently, only $\mathcal{S}_{yx} = \mathcal{S}_{xy}$ appears in the lowest order Eqs. (10)–(13). For simplicity of notation we omit the subscript $xy$ in the following by setting $\mathcal{S} = \mathcal{S}_{xy}$.

In order to calculate $u_x$ we integrate Eq. (10a) twice with respect to $y$ and determine the two integration constants using the boundary conditions Eqs. (4) and (13). Since the reduced pressure $p + \Pi$ is independent of $y$ (see Eq. (10b), a first integration w.r.t. the vertical coordinate from $h$ to $y$ yields together with Eq. (13)

$$(y - h)\, \partial_x (p + \Pi) = \partial_y u_x + \mathcal{S}. \tag{14}$$

Integrating with respect to the vertical coordinate from zero to $y$ gives

$$u_x = \left(\frac{y^2}{2} - y\, h\right) \partial_x \left(p + \Pi\right) - \int_0^y \mathcal{S}(y')\, dy', \tag{15}$$

where we used the substrate boundary condition Eq. (4). Inserting Eq. (15) into the kinematic condition (6) leads to the stochastic thin-film equation. Since the reduced pressure $p + \Pi$ does not depend on $y$, we can evaluate $p + \Pi$ at the film surface and replace $p$ by the boundary condition (11). Rewriting $\Pi$ in terms of the effective interface potential $\Phi$, we get

$$\frac{\partial h}{\partial t} = \partial_x \left\{ \frac{h^3}{3}\, \partial_x \left[\Phi'(h) - \gamma\, \partial_x^2 h\right] + \int_0^h \int_0^y \mathcal{S}(y')\, dy'\, dy \right\}. \tag{16}$$

Integrating the noise term by parts with respect to $y$ entails

$$\frac{\partial h}{\partial t} = \partial_x \left\{ \frac{h^3}{3} \partial_x \left[\Phi'(h) - \gamma\, \partial_x^2 h\right] + \int_0^h (h - y)\, \mathcal{S}(y)\, dy \right\}. \tag{17}$$

The correlator of the nondimensional noise $\mathcal{S}$ is

$$\left\langle \mathcal{S}(x, y, t)\, \mathcal{S}(x', y', t') \right\rangle = 2\, T\, \delta(x - x')\, \delta(y - y')\, \delta(t - t'). \tag{18}$$

In contrast to the thermal noise in the original hydrodynamic equations (2), the noise term in Eq. (17) is multiplied by a function which depends on $h(x,t)$ and therefore on the noise, too. Now the question arises which meaning to give to this product (or the corresponding stochastic integral $\iint (h-y)\,\mathcal{S}\,dy\,dt$). Two common ways of interpretation are Ito and Stratonovich calculus. In Appendix C we show that the corresponding Fokker–Planck Eq. (47) does not depend on the choice of calculus. This is mainly due to the conservative character of the noise in Eq. (17). Therefore Ito and Stratonovich calculus are equivalent here. For simplicity we will use the Ito formalism in the following.

## 2.3. Simplifying the Noise Term

The noise term in Eq. (17) still depends on the vertical coordinate. This is in contradiction to the spirit of long-wave approximation to model film evolution solely in terms of time and planar coordinates. In this section we will show that the following stochastic partial differential equation involving a multiplicative conserved noise term depending only on $x$ and $t$

$$\frac{\partial h}{\partial t} = \partial_x \left\{ \frac{h^3}{3} \partial_x \left[ \Phi'(h) - \gamma\, \partial_x^2 h \right] + \sqrt{\frac{h^3}{3}}\, \mathcal{N} \right\}, \tag{19}$$

with

$$\langle \mathcal{N}(x,t) \rangle = 0 \quad \text{and} \quad \left\langle \mathcal{N}(x,t)\mathcal{N}(x',t') \right\rangle = 2\,T\,q(x-x')\,\delta(t-t'), \tag{20}$$

and $q(x) = \delta(x)$ can be considered identical to Eq. (17) in an appropriate weak sense.[4] Let us make this more precise. Initially, our goal has been to investigate the impact thermal fluctuations have on time-scales of dewetting. Therefore, we are mostly interested in results on the distribution of film profiles at given time-instants $t > 0$. For this reason, we will weakly identify stochastic partial differential equations if the time-evolution of the corresponding distribution functions is identical. In this spirit, we will discretize Eqs. (17) and (19) in space and we will show that the corresponding systems of stochastic differential equations gives rise to the same Fokker–Planck equation, as the spatial discetization parameter tends to zero.

Moreover, we will show that the distribution function which satisfies the detailed balance condition is given by

$$\mathcal{W}_{\text{eq}}[h] = Z^{-1} \exp\left( -\frac{1}{T}\, \mathcal{H}[h] \right) \tag{21}$$

[4] In Eq. (20) we introduce the symmetric correlator $q(x) \geq 0$ because in Sec. 3.2 we will consider also finite correlation lengths in space to study the influence of spatial correlations on the dewetting dynamics.

with the partition function $Z$ (a normalization constant) and the effective interface Hamiltonian

$$\mathcal{H}[h] = \int \Phi(h) + \frac{\gamma}{2} |\partial_x h|^2 \, dx, \tag{22}$$

as expected from thermodynamics.[15] The integrand $\Phi(h) + \frac{\gamma}{2} |\partial_x h|^2$ is the local energy density for the given interface profile $h(x)$.

Note that Eq. (19) has some features in common with stochastic Cahn-Hilliard equations (see for instance[16,17] and the references therein). Both equations are fourth-order parabolic, and they admit for Lyapunov-functionals of a similar structure. In contrast to the stochastic Cahn-Hilliard equations studied so far in the literature, the parabolicity in (19) degenerates. For this reason, analytical techniques to establish the existence of stochastic processes, as presented in[19] and in,[18] cannot be applied.

Let us show now, that the Eqs. (17) and (19) are identical in the sense formulated above. First we rewrite these equations using the Hamiltonian in Eq. (22) and the mobility factor $M(h) = \frac{h^3}{3}$. We get

$$\frac{\partial h}{\partial t} = \partial_x \left[ M(h) \, \partial_x \frac{\delta \mathcal{H}}{\delta h} + \int_0^h (h - y) \, \mathcal{S}(y) \, dy \right] \quad \text{and} \tag{23}$$

$$\frac{\partial h}{\partial t} = \partial_x \left[ M(h) \, \partial_x \frac{\delta \mathcal{H}}{\delta h} + \sqrt{M(h)} \mathcal{N} \right], \tag{24}$$

respectively. Next we discretize in space with lattice constant $a$. The film thickness then becomes a vector $\mathbf{h}$ with $h_i = h(a\, i)$. We replace the integration with respect to $x$ in Eq. (22) by the corresponding Riemann sum

$$\mathcal{H}(\mathbf{h}) = a \sum_i E_i(\mathbf{h}), \tag{25}$$

with the local energy density at lattice site $i$

$$E_i = \Phi(h_i) + \frac{\gamma}{2} \left[ (\nabla^s \cdot \mathbf{h})_i \right]^2. \tag{26}$$

Here we use the symmetric finite difference operator $(\nabla^s \cdot \mathbf{f})_i = \frac{1}{2a} (f_{i+1} - f_{i-1})$. We can also interpret $\nabla^s$ as an infinite matrix with entries $\nabla^s_{ij} = \frac{1}{2a} (\delta_{i,j-1} - \delta_{i,j+1})$ and $\nabla^s \cdot \mathbf{f}$ as the multiplication of the matrix with a vector. In the discretized equation, the variational derivative $\frac{\delta \mathcal{H}}{\delta h}$ becomes the sum over the partial derivatives of $\mathcal{H}(\mathbf{h})$ with respect to $\mathbf{h}$, namely

$$\left( \frac{\delta \mathcal{H}(\mathbf{h})}{\delta \mathbf{h}} \right)_i = \sum_j \frac{\partial E_j(\mathbf{h})}{\partial h_i} = \frac{1}{a} \frac{\partial \mathcal{H}(\mathbf{h})}{\partial h_i}. \tag{27}$$

Note that the variational and the partial derivative of $\mathcal{H}(\mathbf{h})$ with respect to $\mathbf{h}$ differ by a factor $a$.

We discretize the noise terms $\mathcal{S}_i^\ell(t) = \left(\mathcal{S}^\ell(t)\right)_i = \mathcal{S}(a\,i, a\,\ell, t)$ and $\mathcal{N}_i(t) = \left(\boldsymbol{\mathcal{N}}(t)\right)_i = \mathcal{N}(a\,i, t)$. The discretized versions of Eqs. (17) and (19) are then

$$\frac{\partial \mathbf{h}}{\partial t} = \boldsymbol{\nabla}^s \cdot \mathbf{j} \quad \text{with} \tag{28a}$$

$$j_i = M(h_i) \left( \boldsymbol{\nabla}^s \cdot \frac{\delta \mathcal{H}}{\delta \mathbf{h}} \right)_i + \sum_{\ell=0}^{\mathrm{int}(h_i/a)} a\,(h_i - a\,\ell)\,\mathcal{S}_i^\ell \tag{28b}$$

and

$$\frac{\partial \mathbf{h}}{\partial t} = \boldsymbol{\nabla}^s \cdot \mathbf{j} \quad \text{with} \tag{29a}$$

$$j_i = M(h_i) \left( \boldsymbol{\nabla}^s \cdot \frac{\delta \mathcal{H}}{\delta \mathbf{h}} \right)_i + \mathcal{N}_i, \tag{29b}$$

respectively. With $\mathrm{int}(h_i/a)$ we denote the integer part of $h_i/a$. If $h_i$ is not an integer multiple of $a$, we make an error of $\mathcal{O}(a)$ by approximating the integral with respect to $y$ by summation with respect to $\ell$. However, we are interested in the limit $a \to 0$ and we assume here that this error is not important. The discretized correlators are obtained from Eqs. (18) and (20) using $\delta(x - x') \mapsto \frac{1}{a}\delta_{ij}$ etc. and we get

$$\left\langle \mathcal{S}_i^\ell(t)\, \mathcal{S}_j^m(t') \right\rangle = \frac{2\,T}{a^2}\, \delta_{ij}\, \delta_{\ell m}\, \delta(t - t') \tag{30}$$

$$\left\langle \mathcal{N}_i(t)\, \mathcal{N}_j(t') \right\rangle = \frac{2\,T}{a}\, \delta_{ij}\, \delta(t - t'). \tag{31}$$

With this we can write the discretized thin-film Eqs. (28) and (29) as

$$\frac{\partial \mathbf{h}}{\partial t} = \mathbf{F} + \sum_{\ell=0}^{\infty} \boldsymbol{\nabla}^s \cdot \left[ \mathsf{q}_{(\mathbf{h})}^\ell \boldsymbol{\mathcal{S}}^\ell(t) \right] \quad \text{and} \tag{32}$$

$$\frac{\partial \mathbf{h}}{\partial t} = \mathbf{F} + \boldsymbol{\nabla}^s \cdot \left[ \mathsf{q}_{(\mathbf{h})} \boldsymbol{\mathcal{N}}(t) \right], \tag{33}$$

with

$$q^\ell(x) = \begin{cases} 0 & \text{for} \quad \ell > x/a \\ a\,(x - a\,\ell) & \text{for} \quad 0 \le \ell \le x/a \end{cases} \quad \text{and} \tag{34}$$

$$q(x) = \sqrt{\frac{x^3}{3}} = \sqrt{M(x)}. \tag{35}$$

Here we introduce the following notation. For a given scalar function $f(x)$ and two discretized functions (i.e., vectors) $\mathbf{g}$ and $\mathbf{h}$ we define $(\mathsf{f}_{(\mathbf{g})}\mathbf{h})_i = f(g_i)\,h_i$.

With this notation, we can write the deterministic part in Eqs. (32) and (33) as

$$\mathbf{F} = \boldsymbol{\nabla}^s \cdot \left[ \mathsf{M}_{(\mathbf{h})} \left( \boldsymbol{\nabla}^s \cdot \frac{\delta \mathcal{H}}{\delta \mathbf{h}} \right) \right]. \tag{36}$$

In order to calculate the Fokker–Planck equation corresponding to the Eqs. (32) and (33) we need the first and second Kramers–Moyal expansion coefficient. The coefficients for Eq. (33) are given in the literature[20,21] and those for Eq. (32) we calculate in Appendix A. The expansion coefficients of order three and higher are zero because both Eqs. (32) and (33) are Markovian.[20,21]

In Ito calculus the first Kramers–Moyal coefficients of Eqs. (32) and (33) are equal and simply given by the deterministic part

$$\mathbf{D}^{(1)}(\mathbf{h}) = \mathbf{F}(\mathbf{h}), \tag{37}$$

see Eqs. (A.11) and (A.17), respectively. From Eqs. (A.13) and (A.18) we get with $G^{\ell}_{ij}(\mathbf{h}) = \nabla^s_{ij}\, q^{\ell}(h_j)$ and $G_{ij}(\mathbf{h}) = \nabla^s_{ij}\, q(h_j)$ the second coefficients for Eqs. (32) and (33),

$$D^{(2\mathcal{S})}_{ij}(\mathbf{h}) = \frac{T}{a^2} \sum_k \sum_{\ell=0}^{\infty} \nabla^s_{ik}\, q^{\ell}(h_k)\, \nabla^s_{jk}\, q^{\ell}(h_k) \quad \text{and} \tag{38}$$

$$D^{(2\mathcal{N})}_{ij}(\mathbf{h}) = \frac{T}{a} \sum_k \nabla^s_{ik}\, q(h_k)\, \nabla^s_{jk}\, q(h_k), \tag{39}$$

respectively. Since the $\nabla^s_{ik}$ on the right-hand side of Eqs. (38) and (39) are only the components of the symmetric finite difference operator $\boldsymbol{\nabla}^s$, *i.e.*, numbers, and not the operator itself, we can rearrange the factors in the summands to get

$$D^{(2\mathcal{S})}_{ij}(\mathbf{h}) = \sum_k \nabla^s_{ik}\, \nabla^s_{jk}\, \frac{T}{a^2} \sum_{\ell=0}^{\infty} q^{\ell}(h_k)\, q^{\ell}(h_k) \quad \text{and} \tag{40}$$

$$D^{(2\mathcal{N})}_{ij}(\mathbf{h}) = \sum_k \nabla^s_{ik}\, \nabla^s_{jk}\, \frac{T}{a}\, q(h_k)\, q(h_k). \tag{41}$$

Apparently a sufficient condition for the two coefficients to be equal is

$$a\ [q(x)]^2 = \sum_{\ell=0}^{\infty} [q^{\ell}(x)]^2. \tag{42}$$

With the definition in Eqs. (34) and (35) the condition above is satisfied up to order $\mathcal{O}(a)$ since the sum on the right-hand side gives $\frac{a\,x^3}{3} + \frac{a^2\,x^2}{2} + \frac{a^3\,x}{6}$ and the left-hand side is $\frac{a\,x^3}{3}$. In other words, in the continuum limit $a \to 0$ the coefficients are the same and in this sense, the Langevin Eqs. (17) and (19) are equivalent.

With $q(h_k)$ from Eq. (35) we can write the second Kramers–Moyal coefficient as

$$D_{ij}^{(2\mathcal{N})}(\mathbf{h}) = \sum_k \nabla_{ik}^s \frac{T}{a} M(h_k) \nabla_{jk}^s. \tag{43}$$

The Fokker–Planck equation corresponding to Eq. (33) gives the time evolution of the probability density $\mathcal{W}(\mathbf{h})$ of finding $\mathbf{h}$ as solution of Eq. (33) at time $t$

$$\frac{d\mathcal{W}(\mathbf{h})}{dt} = -\frac{\partial}{\partial \mathbf{h}} \cdot \left\{ \left[ \mathbf{D}^{(1)}(\mathbf{h}) - \frac{\partial}{\partial \mathbf{h}} \cdot \mathbf{D}^{(2\mathcal{N})}(\mathbf{h}) \right] \mathcal{W}(\mathbf{h}) \right\}. \tag{44}$$

The discrete analog to the canonical distribution in Eq. (21) is $\mathcal{W}_{\text{eq}}(\mathbf{h}) = Z^{-1} \exp\left(-\frac{1}{T}\mathcal{H}(\mathbf{h})\right)$. In order to show that the canonical distribution satisfies the detailed balance condition, we first demonstrate that the diffusion term (the term $\frac{\partial}{\partial \mathbf{h}} \cdot \mathbf{D}^{(2\mathcal{N})}(\mathbf{h})$ within the square brackets) can be written as $\boldsymbol{\nabla}^s \cdot \mathsf{M}_{(\mathbf{h})} \boldsymbol{\nabla}^s \cdot \frac{\partial}{\partial \mathbf{h}}$. First we have to write the diffusion term with the help of Eq. (43) with indices and apply the product rule for the derivative with respect to $\mathbf{h}$

$$\begin{aligned} &\sum_{j,k} \frac{T}{a} \frac{\partial}{\partial h_j} \nabla_{ik}^s M(h_k) \nabla_{jk}^s \mathcal{W}(\mathbf{h}) \\ &\qquad = \sum_{j,k} \frac{T}{a} \left[ \nabla_{ik}^s \frac{\partial M(h_k)}{\partial h_j} \nabla_{jk}^s \mathcal{W}(\mathbf{h}) + \nabla_{ik}^s M(h_k) \nabla_{jk}^s \frac{\partial \mathcal{W}(\mathbf{h})}{\partial h_j} \right]. \end{aligned} \tag{45}$$

The first term on the right-hand side vanishes because $\frac{\partial M(h_k)}{\partial h_j} = \delta_{jk} \frac{\partial M(h_j)}{\partial h_j}$ is symmetric in $j$ and $k$ while $\nabla_{jk}^s$ is antisymmetric. We then transpose $\nabla_{jk}^s$ in the second term (which produces a minus sign) and we get for the Fokker–Planck equation

$$\frac{d\mathcal{W}(\mathbf{h})}{dt} = -\frac{\partial}{\partial \mathbf{h}} \cdot \left[ \boldsymbol{\nabla}^s \cdot \mathsf{M}_{(\mathbf{h})} \cdot \boldsymbol{\nabla}^s \cdot \left( \frac{\delta \mathcal{H}(\mathbf{h})}{\delta \mathbf{h}} + T \frac{\delta}{\delta \mathbf{h}} \right) \mathcal{W}(\mathbf{h}) \right]. \tag{46}$$

Here we insert the deterministic part from Eq. (36) and make use of $\frac{1}{a}\frac{\partial}{\partial \mathbf{h}} = \frac{\delta}{\delta \mathbf{h}}$, see Eq. (27). In the continuum limit $a \to 0$ the Fokker–Planck equation has the form

$$\frac{d\mathcal{W}[h]}{dt} = -\int \frac{\delta}{\delta h} \left[ \partial_x M(h) \partial_x \left( \frac{\delta \mathcal{H}[h]}{\delta h} + T \frac{\delta}{\delta h} \right) \mathcal{W}[h] \right] dx. \tag{47}$$

A sufficient condition for detailed balance is that the probability current density, i.e., the term in square brackets in Eq. (46) or (47), is identical zero. The reason for this is that the height function $h$ (as well as the discrete $\mathbf{h}$) is an even function, meaning it does not change the sign under time reversal (in contrast to velocities for example), see[21] (Sec. 5.3.5, comment (i)). Using the chain rule for the derivative

of (21) with respect to the film thickness this is obviously the case for the discrete Eq. (46) as well as for the continuum Eq. (47).

## 3. THERMAL NOISE AND TIME-SCALES OF DEWETTING

In this section, we present numerical studies on the effect thermal noise has on dewetting dynamics. Our objective is to give—at the moment on a qualitative level only—numerical evidence for the conjecture that thermal fluctuations may accelerate the transition from a flat, slightly perturbed film to a locally ruptured film. After the first instant of local film rupture, we expect the deterministic terms, i.e., those containing the augmented Laplace pressure $-\nabla_x^2 h + \Phi'(h)$, to dominate the dynamics again—at least under the assumption of moderate noise intensities. This way, we expect noise terms to overcome the discrepancies in the ratio of dewetting time-scales between experiment and deterministic numerical studies which were observed in.[5] Before presenting our numerical results, let us formulate a numerical scheme for the computation of sample paths of the stochastic process related to the stochastic thin-film Eq. (19).

The particular structure of the noise term (convective, multiplicative) as well as the degeneracies and singularities inherent in the deterministic thin-film equation make the discretization of Eq. (19) an intricate problem. Although the deterministic equation is fourth-order and comparison principles do not hold, rigorous mathematical results show that globally non-negative solutions exist, provided initial data are non-negative, see.[3,22–25] This is a consequence of the mobility $M(h)$ vanishing at zero. To guarantee *non-negativity* properties of discrete solutions, it is crucial that the numerical scheme mimics the degeneracy of the mobility (see our choice of harmonic integral means in Appendix B). If the effective interface potential is $+\infty$ at zero film thickness with sufficiently high order, even a pathway to strict *positivity* opens up. To establish this, it is sufficient to split $\Phi$ into a sum of a non-negative convex and a concave component and to discretize the first one implicitly, the second one explicitly. Finally, as the stochastic process $\mathcal{N}(x,t)$ appears inside a convective term, numerical diffusion becomes an issue. We use upwinding concepts to minimize this effect.

To have a perspective of numerical analysis, we will formulate $\mathcal{N}(x,t)$ in the framework of $Q$-Wiener processes. It turns out that the corresponding structure carries over to the discrete setting.

Summing up, the plan of this section is as follows. First, we formulate Eq. (19) as an initial-boundary-value problem and we recall the essentials of the concept of $Q$-Wiener processes. We transfer this concept to a discrete setting and formulate a scheme for the convective term $\partial_x[\sqrt{M(h)}\mathcal{N}(x,t)]$. For the reader's convenience, the main ideas for the efficient discretization of the deterministic thin-film equation are summarized in Appendix B. At the end of Sec. 3.1, we arrive at a numerical scheme. In Sec. 3.2 we present first numerical results.

### 3.1. A Numerical Scheme for the Stochastic Thin-Film Equation

In this section, we consider an initial-boundary-value problem related to the stochastic thin-film Eq. (19). In particular, we give a meaning to the stochastic process $\mathcal{N}(x,t)$ in terms of $Q$-Wiener processes. This formalism at hand we will formulate a numerical method subsequently. We will consider Eq. (19) on the space-time cylinder $\Omega_{\mathcal{T}} := (0,L)\times(0,\mathcal{T})$ subjected to spatially periodic boundary conditions. We choose non-negative initial data with finite energy. We require the correlation function $q$ introduced in Eq. (20) to be $L-$periodic. Recall that it is even and non-negative, too. For simplicity[5] we assume $q$ to be continuous. It is well known (see, e.g.[26] or[27]) that space-time noise $\mathcal{N}(x,t)$ satisfying Eq. (20) can be written as the formal time-derivative of the $Q$-Wiener process $W(x,t)$, namely

$$\mathcal{N}(x,t) = \frac{\partial W}{\partial t}(x,t) = \sum_{k=-\infty}^{+\infty} \lambda_k \,\dot{\beta}_k(t)\, g_k(x). \tag{48}$$

The $\beta_k$, $k\in\mathbb{Z}$, form a family of mutually independent Brownian motions with respect to time and the dot denotes the time-derivative. $\lambda_k^2$, $k\in\mathbb{Z}$, are the eigenvalues of the Hilbert-Schmidt operator $Q$

$$(Qf)(x) := 2\,T\int_0^L q(y-x)\,f(y)\,dy \tag{49}$$

corresponding to the complete system of orthonormal eigenfunctions

$$g_k(x) := \begin{cases} \sqrt{\frac{2}{L}}\,\cos(2\pi\,k\,\frac{x}{L}) & \text{for} \quad k\in\mathbb{N} \\ \sqrt{\frac{1}{L}} & \text{for} \quad k=0 \\ \sqrt{\frac{2}{L}}\,\sin(2\pi\,k\,\frac{x}{L}) & \text{for} \quad -k\in\mathbb{N}. \end{cases} \tag{50}$$

Since $q$ is real and symmetric we have $\lambda_k^2 = \lambda_{-k}^2 \geq 0$.

For the discretization of Eq. (19), a number of side conditions have to be respected. To enhance the numerical performance, it is recommended to solve the equation in a finite-element/finite-volume setting. An approach based on Fourier-series (suggested by the trigonometric eigenfunctions of $Q$ in Eq. (50)) has the disadvantage that the nonlinearities inherent in Eq. (19) give rise to linear systems involving full matrices. In addition, it is not known whether a Fourier-approach

[5] Since only spatially discrete noise enters the numerical simulations, assuming $q(x)$ to be continuous does not mean any restriction—even not in the case of discrete approximations of white noise. Just assume supp $q$ to be sufficiently small.

allows for non-negativity results for discrete solutions—in particular if the effective interface potential is not $+\infty$ at $h = 0$.

We describe now the ingredients of the numerical scheme we are going to use. For $N \in \mathbb{N}$ we are given a uniform discretization of the interval $\Omega = [0, L]$ with grid parameter $a := \frac{L}{N}$ and nodal points $x_i := i\,a$, with $i = 0, \ldots, N$. Corresponding to this, we consider the periodic linear finite-element space

$$V_{per}^N := \{v \in H_{per}^1(\Omega) : v|_{(x_i, x_{i+1})} \text{ is linear } \forall\, i = 0, \ldots, N-1\}.$$

Here, $H_{per}^1(\Omega) := \{v \in H_{loc}^1(\mathbb{R}) : v(x) = v(x + L) \text{ a.e. in } \mathbb{R}\}$ where $H_{loc}^1(\mathbb{R})$ is the usual Sobolev space of measurable, locally square-integrable functions which have locally square-integrable weak derivatives of first order. A basis of $V_{per}^N$ is given by functions $\phi_j \in V_{per}^N$ satisfying $\phi_j(x_i) = \delta_{ij}$, $i, j = 1, \ldots, N$. We introduce the nodal projection operator $\mathcal{I}_N : H_{per}^1(\Omega) \to V_{per}^N$ which maps $u \in H_{per}^1(\Omega)$ to the unique element $\mathcal{I}_N u \in V_{per}^N$ satisfying $u(x_i) = \mathcal{I}_N u(x_i)$ for all $i = 0, \ldots, N$. The graph of $\mathcal{I}_N u$ is a polygon through the points $(x_i, u(x_i))$, $i = 0, \ldots, N$. This way, we may define the lumped masses scalar product

$$(\Theta, \Psi)_N := \int_0^L \mathcal{I}_N(\Theta \cdot \Psi). \tag{51}$$

The diagonal and positive definite lumped mass matrix $M_N$ is given by $(M_N)_{ij} = (\phi_i, \phi_j)_N = a\,\delta_{ij}$, and $L_N$ stands for the stiffness matrix $(L_N)_{ij} = (\nabla\phi_i, \nabla\phi_j)$, where we write $(u, v)$ for the usual $L^2-$scalarproduct on $\Omega$.

In the following $H^n \in V_{per}^N$ denotes the discrete approximation to the solution $h(x, t_n)$ of Eq. (19) after $n$ time steps. Introducing the coefficient vector $\bar{H} \in \mathbb{R}^N$, we can write $H^n = \sum_{i=1}^N \bar{H}_i^n\,\phi_i$.

**Discretization of the stochastic part.** Let us concentrate now on the stochastic part of Eq. (19). Ignoring for a moment the deterministic terms on the right-hand side, we are formally left with the scalar conservation law

$$\frac{\partial h}{\partial t} = \partial_x \left[\sqrt{M(h)}\mathcal{N}(x, t)\right]. \tag{52}$$

We discretize this equation in two steps. Formulating first a discretization of the noise term, we insert it in the second step into a standard upwind scheme for the convective term.

In Eq. (48), the noise term is written as an infinite sum of mutually independent stochastic processes. In the discrete setting, the number of processes is to be chosen identical to the dimension of $V_{per}^N$. Therefore, we need only $N$ processes, and we discretize the correlation function in the following way. For each nodal

point $i = 0, \ldots, N$, we consider

$$q_{Ni} := a^{-1} \int_{x_i - \frac{a}{2}}^{x_i + \frac{a}{2}} q(x)\, dx \tag{53}$$

as the discrete substitute of $q$. By periodicity of $q$, we have $q_{N0} = q_{NN}$. Extending $q_{Ni}$, $i = 0, \ldots, N$, to a mapping $q : \mathbb{Z} \times \mathbb{Z} \to \mathbb{R}_0^+$ according to the rules

$$q_{ij} = q_{i+l\, j+l} \quad \text{and} \quad q_{i+N\, j} = q_{i\, j+N} = q_{ij} \quad \text{foreach} \quad i, j, l \in \mathbb{Z}, \tag{54}$$

we get a discrete substitute for the Hilbert-Schmidt operator $Q$. It is the operator $Q_N : \mathbb{R}^N \to \mathbb{R}^N$ which for $y \in \mathbb{R}^N$ is defined as

$$(Q_N\, y)_i := 2\, T\, a \sum_{j=1}^{N} q_{ij}\, y_j. \tag{55}$$

Note in particular that $Q_N = 2\, T\, \mathrm{Id}_{\mathbb{R}^N}$ if $q|_{(-L/2, L/2)}$ is a continuous approximation of $\delta(x)$ supported in $(-a/2, a/2)$. The following lemmata can easily be proven.

**Lemma 3.1.** *Let $N \in \mathbb{N}$ be an odd number. For $k \in \{-\frac{N-1}{2}, \ldots, \frac{N-1}{2}\}$ consider $\mathbf{g}^k \in \mathbb{R}^N$ defined as $g_i^k := g_k(x_i)$, $i = 1, \ldots, n$. Then there exist numbers $\sigma_k^2(N)$, $k \in \{-\frac{N-1}{2}, \ldots, \frac{N-1}{2}\}$, with $\sigma_{-k}^2(N) = \sigma_k^2(N)$, such that*

$$Q_N \cdot \mathbf{g}^k = \sigma_k^2(N)\, \mathbf{g}^k \qquad \forall\, k \in \left\{-\frac{N-1}{2}, \ldots, \frac{N-1}{2}\right\}. \tag{56}$$

*The $\mathbf{g}^k$, $k = -\frac{N-1}{2}, \ldots, \frac{N-1}{2}$ form an orthonormal basis of $\mathbb{R}^N$ with respect to the scalar product $\langle \mathbf{x}, \mathbf{y} \rangle_N := a \sum_{i=1}^N x_i y_i$.*

*If $q \in L^2(0, L)$ with $\lambda_k^2$, $k \in \mathbb{Z}$, the eigenvalues of the corresponding Hilbert-Schmidt operator $Q$, then we have for each $k \in \mathbb{Z}$*

$$\lim_{N \to \infty} \sigma_k^2(N) = \lambda_k^2. \tag{57}$$

**Lemma 3.2.** *Let $N \in \mathbb{N}$ be an odd number. For $k \in \{-\frac{N-1}{2}, \ldots, \frac{N-1}{2}\}$, the functions $\mathcal{I}_N g_k$ form an orthonormal basis of $V_{per}^N$ with respect to the lumped masses scalar product $(\cdot, \cdot)_N$.*

For a mutually independent family of Brownian motions $\beta_k$ with respect to time, $k \in \{-\frac{N-1}{2}, \ldots, \frac{N-1}{2}\}$, we consider the spatially discretized $Q_N$-Wiener process $W_a(x, t)$ and the corresponding spatially discrete noise

$$\mathcal{N}_a(x, t) := \frac{\partial W_a}{\partial t}(x, t) = \sum_{k=-\frac{N-1}{2}}^{\frac{N-1}{2}} \sigma_k(N)\, \dot{\beta}_k(t)\, \mathcal{I}_N g_k(x), \tag{58}$$

for which we can easily establish the following results.

**Lemma 3.3.** *For times $t, s \in [0, \mathcal{T}]$, a position $x \in [0, L]$, and node numbers $i, j \in \{1, \dots, N\}$ we have $\langle \mathcal{N}_a(x,t)\rangle = 0$ and $\langle \mathcal{N}_a(x_i,t)\mathcal{N}_a(x_j,s)\rangle = 2\,T\,\delta(t-s)\,q_{ij}$.*

Note that this way the structure of $Q-$Wiener-processes is transferred to the discrete setting. In fact, (49) has its analogue in (55), the eigenfunctions $\mathcal{I}_N g_k$ are orthonormal w.r.t. the lumped masses scalar product, and the properties stated in (20) correspond to those stated in Lemma 3.3.

To discretize the time-Wiener-processes in the framework of Ito-calculus, we replace $\dot\beta_k(t_n)$ at a time-step $t_n$ by the forward difference quotient

$$\frac{\beta_k(t_{n+1}) - \beta_k(t_n)}{t_{n+1} - t_n}. \tag{59}$$

The difference $\beta_k(t_{n+1}) - \beta_k(t_n)$ is normal distributed and the variance is given by the time-increment $\tau_n := t_{n+1} - t_n$. On the discrete level, we approximate the difference quotient (59) by $\frac{\mathcal{N}_k^n}{\sqrt{\tau_n}}$, $k \in \{-\frac{N-1}{2}, \dots, \frac{N-1}{2}\}$. Here, $n$ is the index of time-stepping, and $\mathcal{N}_k^n$ are computer generated random numbers which are approximately $N(0,1)$–distributed. Altogether, the space-time-discrete noise term is given by

$$\mathcal{N}_{a,\tau_n}^n(x) := \frac{1}{\sqrt{\tau_n}} \sum_{k=-\frac{N-1}{2}}^{\frac{N-1}{2}} \sigma_k(N)\,\mathcal{N}_k^n\,\mathcal{I}_N g_k(x). \tag{60}$$

By construction, both $\mathcal{N}_a(x,t)$ and $\mathcal{N}_{a,\tau_n}^n(x)$ are $L$-periodic in $x$.

The second ingredient is an upwind discretization for the scalar conservation law in Eq. (52) subjected to periodic boundary conditions for both $\mathcal{N}$ and $h$ which is inspired by.[28] For $j = 0, \dots, N-1$ we introduce

$$\bar{\mathcal{N}}_{j+\frac12}^n := a^{-1} \int_{x_j}^{x_{j+1}} \mathcal{N}_{a,\tau_n}^n(x)\,dx \tag{61}$$

and we abbreviate

$$M_0(h) := M(\max(0,h)). \tag{62}$$

Then the scheme reads as follows. Given a function $H^0 := \sum_{j=1}^N \bar H_j^0 \phi_j$, find for $n \in \mathbb{N}$ iteratively vectors $\bar H^n \in \mathbb{R}^N$ which satisfy

$$\bar H_j^{n+1} = \bar H_j^n - \frac{\tau_n}{a}\left(\bar{\mathcal{N}}_{j+\frac12}^n \mathcal{M}_{j+\frac12}^n - \bar{\mathcal{N}}_{j-\frac12}^n \mathcal{M}_{j-\frac12}^n\right) \tag{63}$$

with

$$\mathcal{M}_{j+1/2}^n := \begin{cases} \sqrt{M_0(\bar H_j^n)} & \text{if} \quad \bar{\mathcal{N}}_{j+\frac12}^n \ge 0, \\ \sqrt{M_0(\bar H_{j+1}^n)} & \text{if} \quad \bar{\mathcal{N}}_{j+\frac12}^n < 0. \end{cases} \tag{64}$$

Using the notation

$$\left[\partial_{EO}^{N}\left(\sqrt{M_0(\bar{H}^n)},\mathcal{N}_{a,\tau_n}^{n}(\cdot)\right)\right]_j = a^{-1}\left\{\bar{\mathcal{N}}_{j+\frac{1}{2}}^{n}\mathcal{M}_{j+\frac{1}{2}}^{n}-\bar{\mathcal{N}}_{j-\frac{1}{2}}^{n}\mathcal{M}_{j-\frac{1}{2}}^{n}\right\}, \tag{65}$$

we may abbreviate

$$\bar{H}^{n+1}=\bar{H}^n-\tau_n\,\partial_{EO}^{N}\left(\sqrt{M_0(\bar{H}^n)},\mathcal{N}_{a,\tau_n}^{n}(\cdot)\right). \tag{66}$$

**The full time stepping scheme.** Combining the scheme for the convective part (66) with the scheme for the fourth-order equation from Eq. (B.5), we end up with the full time-stepping scheme for Eq. (19)

$$\bar{H}^{n+1}+\frac{\tau_n}{a}\,L_N^M(\bar{H}^{n+1})\cdot\left[\frac{1}{a}\,L_N\cdot\bar{H}^{n+1}+\Phi_+'(\bar{H}^{n+1})+\Phi_-'(\bar{H}^n)\right] = \bar{H}^n+\tau_n\,\partial_{EO}^{N}\left(\sqrt{M_0(\bar{H}^n)},\mathcal{N}_{a,\tau_n}^{n}(\cdot)\right). \tag{67}$$

$L_N^M$ is the mobility weighted stiffness matrix and $\Phi_+$ is the non-negative and convex part of the effective interface potential while $\Phi_-$ is the concave rest term, see Appendix B.

In the original equation Eq. (19), the function under the square root in the prefactor of the noise term is the mobility. As shown in Sec. 2.3 this is necessary if one wants the stationary distribution to be given by the Boltzmann weight. The prefactor of the noise term in Eq. (67) is not the square root of the discrete mobility $M_\sigma$ defined in Eq. (B.3). This is due to the fact that it is not clear whether an upwind scheme can be constructed using the discretized mobility. Note however that the difference between the different mobilities is small and of order $a$.

## 3.2. Numerical Results

In physical experiments on the dewetting of liquid films on planar surfaces, usual three different time-scales can be observed. The first one is characterized by the time which is needed to pass from an initially nearly flat film to the first local rupture event. Much smaller is the time-scale of droplet formation which covers the time interval from the first rupture instant to the formation of a metastable collection of droplets connected by ultra-thin films. The third time-scale is that one of coarsening–it is by far the largest one (see e.g.[29] for further details). In this subsection, we give numerical evidence for our conjecture that thermal

**Fig. 2.** Snapshots at times $t = 10,\ 12,\ 13,\ 14,\ 15,\ 15.5,\ 15.75,\ 16$ for the deterministic thin-film equation. Discretisation parameters are the grid spacing $a = 2^{-9}\ L$ and time step $\tau = a^{5/2}$.

fluctuations may accelerate film rupture, i.e. diminish the ratio

$$\frac{\text{rupture time-scale}}{\text{droplet-formation time-scale}}.$$

To this scope, we perform a number of numerical experiments on $\Omega = (0, L)$, $L = 15$ and we choose the effective interface potential $\Phi(h) := \frac{1}{30} \cdot h^{-3} - \frac{1}{2} \cdot h^{-2}$. Generically, our choice of correlation function $q$ (cf. (20)) restricted to $(-L/2, L/2)$ is

$$q(x, l_c) := \begin{cases} Z^{-1} \cdot \exp\left( -\frac{1}{2} \sin^2(\frac{\pi x}{L}) \frac{L^2}{l_c^2} \right) & \text{if} \quad l_c > 0 \\ \delta(x) & \text{if} \quad l_c = 0. \end{cases}$$

Here, $Z$ is chosen such that $\int_0^L q(x, l_c)\, dx = \sqrt{2T}$. Note that $l_c$ denotes the correlation length.We probe the influence of characteristic noise parameters like intensity $T$ and correlation length on the dewetting dynamics. As a first step towards studying the properties of the scheme, we monitor the dependence of the results on various discretization parameters, too. It turns out that the effect of noise on the *droplet-formation time-scale* is negligible. In that regime, the fourth-order operator governs the evolution. In contrast, the *rupture time-scale* is strongly affected by noise effects and becomes smaller monotoneously with increasing noise intensity and decreasing correlation length.

To provide a qualitative picture, Figs. 2 and 3 show snapshots of the deterministic process and of a sample path of the stochastic process under moderate noise intensity, respectively. Note that the time of first rupture decreases from 15.5 (deterministic) to 2.98 (stochastic) whereas the time span needed to form droplets after the first rupture event remains approximately the same. In fact, a closer look

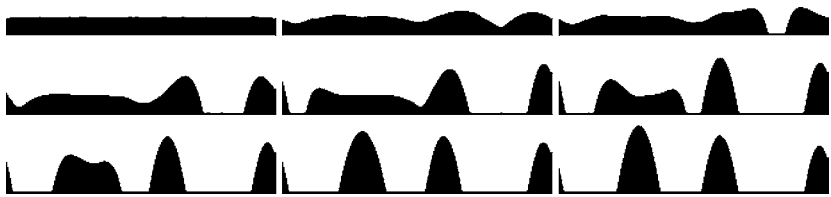

**Fig. 3.** Snapshots at times $t = 0.025,\ 2.9,\ 3.0,\ 3.1,\ 3.2,\ 3.3,\ 3.4,\ 3.5,\ 4.0$ for the stochastic TFE with correlation length $l_c = 0$ and noise strength $T = 0.00125$. The discretisation parameters, initial conditions and spatial domain size are the same as in Figure 2.


**Fig. 4.** Film roughness in terms of correlation length $l_c$: Local snapshots of the film surface at times $t = 0.025$ and 0.05 for noise strength $T = 4.05 \times 10^{-3}$ and $l_c = 0,\ 0.5,\ 1$ (from left to right). Discretization with $a = 2^{-9}L, \tau = a^2$. For the three simulations the same sequence of random numbers have been used.

at the numerical results reveals that the parabolic character of single droplet profiles is essentially not affected by the noise. This is in contrast to the planar film for which the roughness of the film surface reflects the correlation length of the noise (see Fig. 4 for snapshots of sample paths for processes corresponding to different correlation lengths).

In general, this effect is the stronger, the stronger the noise intensity is. Figure 5 provides histograms of the time of first rupture events for $K = 20$ realizations of stochastic processes with intensity factors $T = 5 \times 10^{-5}$ and $T = 1.25 \times 10^{-3}$, respectively. Similarly, the noise induced acceleration is enhanced for decreasing correlation length and for increasing noise intensity as shown in Table I.

As both the practical and the analytical aspects of stochastic thin-film numerics constitute a vast "terra incognita," in a first step it seems necessary to scrutinize whether our choice of discretization parameters with respect to time or to space might affect the first rupture instant. For white noise, Table II gives first indication of the effects the spatial discretization has on rupture times. For a fixed time discretization $\tau = a^{5/2}$ and various noise intensities there is no statistically significant effect of spatial discretization on rupture times. In particular, this effect is negligible compared to the effects noise intensities have on rupture. Similarly,

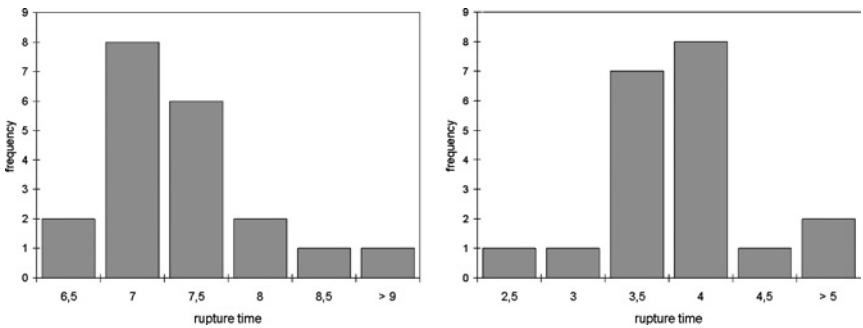


**Fig. 5.** Statistics of first-rupture time for white noise driven thin-film flow ($l_c = 0$): Computation of 20 sample paths for $T = 5 \times 10^{-5}$ (left, mean value and standard deviation are $(\mu, \sigma) = (7.1, 0.4)$) and $T = 1.25 \times 10^{-3}$ (right, $(\mu, \sigma) = (3.6, 0.4)$) respectively. Discretization with $a = 2^{-8}L, \tau = a^2$.

**Table I. First-rupture time in terms of noise intensity and correlation length**

| $T\backslash l_c$ | 0 | 0.25 | 0.5 | 1 |
|---|---|---|---|---|
| 0 | 16.5 | 16.5 | 16.5 | 16.5 |
| $5.00 \times 10^{-5}$ | 8.9 | 10.0 | 10.2 | 10.3 |
| $4.50 \times 10^{-4}$ | 6.5 | 7.8 | 8.0 | 8.2 |
| $1.25 \times 10^{-3}$ | 5.2 | 6.6 | 6.7 | 7.0 |
| $2.45 \times 10^{-3}$ | 4.5 | 5.7 | 5.8 | 6.1 |
| $4.05 \times 10^{-3}$ | 3.9 | 5.1 | 5.3 | 5.5 |

*Note.* Average over two sample paths each. Discretization $a = 2^{-9}L$, $\tau = a^2$.

for various noise intensities and a fixed spatial grid parameter $a = 2^{-9}L$, Fig. 6 indicates that the particular choice of time-increments does not have significant impact on rupture times. These findings are further supported by formal integral estimates based on Ito's formula which will enter future work[30] on the existence of a.s. non-negative processes solving the stochastic thin-film equation.

## 3.3. Physical Relevance

In this subsection, we sketch a scaling argument which indicates that the relative change of dewetting time-scales caused by thermal fluctuations has the right order of magnitude to resolve the discrepancies between physical experiment and deterministic simulation observed in.[5] Since presently we do not have a numerical scheme at our disposal for the multi-dimensional SPDE which would allow for a dimensionalized comparison with the physical experiment, we estimate noise amplitudes based on the data of[5] and compare them with our results in

**Table II. Monitoring the scheme for white noise driven thin-film flow ($l_c = 0$): Mean rupture time and standard deviation (averaged over 6 sample paths each) in terms of spatial discretization parameters $a = 2^{-g}$ and various noise intensities**

| $T\backslash g$ | 7 | 8 | 9 |
|---|---|---|---|
| 0 | 13.5 | 15.7 | 15.5 |
| $5.00 \times 10^{-5}$ | $7.3 \pm 1.0$ | $7.1 \pm 0.9$ | $6.0 \pm 0.8$ |
| $1.25 \times 10^{-3}$ | $3.9 \pm 1.0$ | $3.1 \pm 0.5$ | $2.4 \pm 0.6$ |
| $4.05 \times 10^{-3}$ | $2.5 \pm 0.5$ | $1.6 \pm 0.4$ | $1.4 \pm 0.5$ |

*Note.* Time discretization $\tau = a^{5/2}$. All runs were started with same initial data.

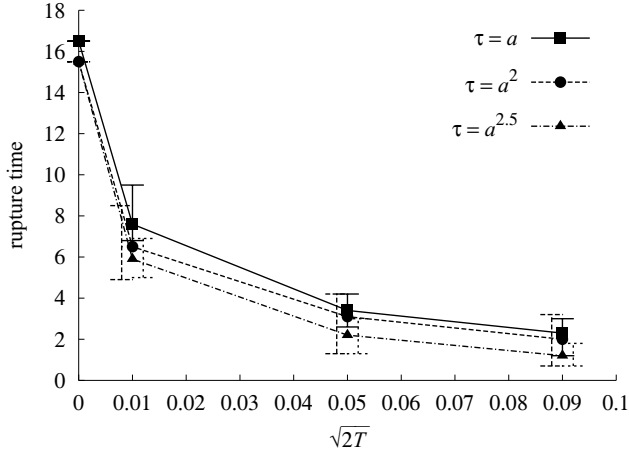


**Fig. 6.** Monitoring the scheme for white noise driven thin-film flow ($l_c = 0$): Mean rupture time (averaged over six sample paths each) as a function of various noise intensities $\sqrt{2\,T}$ for several time discretizations. Errorbars indicate the standard deviation. For $\tau = a^2$ and $\tau = a^{2.5}$ errorbars were shifted to the left and right by 0.002, respectively, for better visibility. Spatial discretization $a = 2^{-9}L$. All runs were started with same initial data.

Subsec. 3.2. So let us return to dimensionalized quantities

$$\eta\,\frac{\partial h}{\partial t} = \partial_x \left\{ \frac{h^3}{3}\,\partial_x \left[\Phi'(h) - \gamma\,\nabla_x^2 h\right] + \sqrt{\frac{h^3}{3}}\,\mathcal{N} \right\} \tag{68}$$

and

$$\langle \mathcal{N}(x,t)\,\mathcal{N}(x',t')\rangle = 2\,k_B\,T\,\eta\,\delta(x-x')\,\delta(t-t'). \tag{69}$$

Here, the unit of the noise $\mathcal{N}$ is $\frac{\eta U}{\sqrt{d}}$. For the sake of clarity, we use the tilde again to distinguish between dimensionalized and non-dimensionialized quantities here. In order to estimate the amplitude $\tilde{T} = \frac{k_B\,T\,d}{\eta\,U\,\lambda^3}$ of the noise, we consider the system studied in,[5] i.e., a polystyrene (PS) film of thickness $d \approx 4$ nm on silicon dioxide. In this case, the thin liquid film is linearly unstable and the characteristic lateral length scale is given by the dispersive capillary length $\lambda = 4\sqrt{\frac{\pi^3\,\gamma\,d^4}{A}}$, which is the most unstable mode in a linear stability analysis of the deterministic part of Eq. (68). With the Hamaker constant $A \approx 2 \times 10^{-20}$ nm and the surface tension coefficient $\gamma \approx 3 \times 10^{-2}$ N/m we have $\lambda \approx 400$ nm. The Hamaker constant determines the disjoining pressure $\Pi(h) = -\frac{A}{6\,\pi\,h^3}$ if we neglect the short-ranged part of the potential. The viscosity is $\eta \approx 1200$ Ns/m$^2$. In the deterministic part of Eq. (68) there are two terms which can drive the flow, the disjoining pressure and the surface tension. The flow associated with each part is of the order of $dU$ and

from this we derive two characteristic velocities, namely $U_\Pi = \frac{A}{6\pi d\lambda\eta} \approx 0.6$ nm/s and $U_\gamma = \frac{d^3\gamma}{3\lambda^3\eta} \approx 8 \cdot 10^{-3}$ nm/s, respectively. We have to take the larger of the two velocities and therefore $U \approx 0.6$ nm/s. According to Eq. (8) with this choice of $U$ the nondimensional disjoining pressure has no free parameter $\tilde{\Pi}(\tilde{h}) = -\frac{1}{\tilde{h}^3}$ and the noise amplitude is given by $\tilde{T} = \frac{3k_BT}{8\pi^2 d^2\gamma}$, i.e., independent of the Hamaker constant and the viscosity. This result is in fact independent of the form of the disjoining pressure and also holds if the short-ranged part is included. The experiments were performed at $T = 53^\circ$C and we have $k_B T \approx 4.5 \times 10^{-21}$ Nm. This leads to $\tilde{T} \approx 4 \times 10^{-4}$. The noise induced current is therefore about two orders of magnitude smaller than the current induced by the disjoining pressure. With the rescaling in Eq. (8) and the choice of $\lambda$ and $U$ from above the nondimensional surface tension coefficient is $\tilde{\gamma} = \frac{3}{8}$. Now observe (cf. Figs. 2, 3, and Table I) that noise intensities of order $\tilde{T} \sim 10^{-4}$ diminish the ratio between *rupture time-scale* and *droplet-formation time-scale* in our first numerical experiments by a factor 5. Hence, our results would be of the right order of magnitude to resolve the discrepancies with respect to time-scales observed in Fig. 1 of.[5] The first image shows the film just after rupture while the last one gives a rough estimate for the droplet formation time.

## 4. CONCLUSIONS

In this paper, we derived a stochastic version of the thin-film equation based on the lubrication approximation for incompressible stochastic hydrodynamic equations.[7] We demonstrated its thermodynamic consistency, in particular with the equilibrium distribution of film thickness. The derivation of the SPDE was presented in one space dimension, it can, however, be generalized to the higher dimensional setting in a straightforward way, and we get

$$\frac{\partial h}{\partial t} = \nabla \cdot \left\{ \frac{h^3}{3} \nabla \left[ \Phi'(h) - \gamma \nabla^2 h \right] + \sqrt{\frac{h^3}{3}} \mathcal{N}(t) \right\}, \tag{70}$$

with $\langle \mathcal{N}(\mathbf{r}, t) \rangle = 0$ and $\langle \mathcal{N}_i(\mathbf{r}, t) \mathcal{N}_j(\mathbf{r}', t') \rangle = 2T \delta_{ij} \delta(\mathbf{r} - \mathbf{r}') \delta(t - t')$. This stochastic equation can be used to investigate the influence thermal fluctuations have on (de)wetting dynamics of thin liquid films which has been studied extensively in the last decades, but theoretically solely by deterministic dynamical equations. However, thermal noise gains a more and more important role the smaller the system size becomes.

Recent studies of thin film evolution indicate that thermal noise influences characteristic time-scales of the dewetting process of linearly unstable thin films.[5] For an experimental model system the measured film morphology has been compared quantitatively to the numerical solution of the deterministic thin film equation with measured microscopic system parameters such as the substrate

potential $\Phi$ and the surface tension $\gamma$. One observes the same spatial patterns in the experiment as well as in the simulation but the time scales do not match.

The numerical solutions presented here are based on a finite-volume scheme for the discretization of the stochastic thin-film Eq. (70) in one dimension. Our results cannot be compared to experiments directly but they indicate that thermal noise accelerates the initial dewetting process of the film rupture while leaving the time-scale of droplet formation unchanged.

This might resolve the reported discrepancies between experiments and deterministic simulations in.[5] In addition, the conserved noise term in the stochastic thin film Eq. (70) changes the spectrum of fluctuations as compared to the deterministic dynamics considerably. This prediction seem to be confirmed in recent AFM measurements of the initial states of dewetting of thin polymer films.[31] Thus, from a physical point of view, it is desirable to develop higher-dimensional schemes for Eq. (70) and to compare dimensionalized numerical simulations with physical experiments of thin films.

As a consequence of the results presented here, also a number of interesting mathematical questions arise. It remains to investigate existence (and uniqueness) of a stochastic process solving (70), and it will be an issue not only for physical reasons to prove non-negativity of the paths almost surely. Related to this question is the problem of analyzing the scheme proposed in Sec. 3, the qualitative behaviour of solutions as well as their convergence properties in the limit of vanishing discretization parameters. It might also be inspiring to provide rigorous estimates for the acceleration effect thermal fluctuations have on dewetting dynamics.

In the course of miniaturisation of electronic and microfluidic devices a fully quantitative description of Newtonian liquids at surfaces are essential and requires quantitative stochastic modelling of ultrathin film dynamics as well as mathematically well-controlled numerical schemes as presented here.

## APPENDIX A. MANY STOCHASTIC PROCESSES PER DEGREE OF FREEDOM

The stochastic thin-film Eq. (32) differs from the stochastic differential equations as discussed in[20,21] in that there are more stochastic processes $\mathcal{S}_i^\ell(t)$ than dependent variables $h_i(t)$. However, all the $\mathcal{S}_i^\ell(t)$ are Gaussian random variables with zero mean and they are $\delta$-correlated, see Eq. (30). In this appendix we will calculate the Fokker–Planck equation corresponding to such a stochastic differential equation.

With $G_{ij}^\ell(\mathbf{h}) = \nabla_{ij}^s q^\ell(h_j)$ we can write Eq. (32) in the form

$$\frac{d\mathbf{h}}{dt} = \mathbf{F}(\mathbf{h}) + \sum_{\ell=0}^{\infty} \mathbf{G}^\ell(\mathbf{h}) \cdot \boldsymbol{\mathcal{S}}^\ell(t), \tag{A.1}$$

with

$$\langle \boldsymbol{\mathcal{S}}^{\ell}(t)\rangle = 0, \quad \left\langle \mathcal{S}_i^{\ell}(t)\,\mathcal{S}_j^{m}(t)\right\rangle = 2\,T\,\delta_{ij}\,\delta_{\ell m}\,\delta(t-t'), \tag{A.2}$$

and $T = \tau/a^2$. The following arguments do not depend on the explicit form of $\mathbf{F}$ and $\mathbf{G}^{\ell}$ and both can be generalized to $\mathbf{F}$ and $\mathbf{G}^{\ell}$ which depend on time explicitly. However, we require that both can be expanded in a Taylor series around any $\mathbf{h}$. We are interested in the time evolution of the probability $\mathcal{W}(\mathbf{h}, t)$ to find the $\mathbf{h}$ at time $t$. This time evolution is in general given by the Kramers–Moyal expansion [20] (Eq. (4.86))

$$\frac{\partial \mathcal{W}(\mathbf{h}, t)}{\partial t} = \sum_{n=1}^{\infty} \sum_{i_1,\ldots,i_n} \frac{(-1)^n\,\partial^n}{\partial h_{i_1}\ldots\partial h_{i_n}} D^{(n)}_{i_1,\ldots,i_n}(\mathbf{h})\,\mathcal{W}(\mathbf{h}, t), \tag{A.3}$$

with the Kramers–Moyal expansion coefficients

$$D^{(n)}_{i_1,\ldots,i_n}(\mathbf{h}) = \frac{1}{n!}\lim_{\Delta t\to 0}\frac{1}{\Delta t}\left\langle \left[h_{i_1}(t+\Delta t) - h_{i_1}(t)\right]\ldots\left[h_{i_n}(t+\Delta t) - h_{i_n}(t)\right]\right\rangle. \tag{A.4}$$

If the Kramers–Moyal expansion coefficients are zero for $n > 2$ one calls the Kramers–Moyal expansion Eq. (A.3) Fokker–Planck equation. We will see that this is indeed the case for Eq. (A.1) and we will calculate the first and second expansion coefficient. For general $G^{\ell}_{ij}(\mathbf{h})$ the second coefficient depends on the choice of stochastic calculus. In this appendix we use Ito calculus but the following calculations can be generalized to Stratonovich calculus easily.

In order to calculate the Kramers–Moyal coefficients we use the method outlined in [20] (Sec. 3.4) for the simpler case when there are not more noise terms than dependent variables. First we write Eq. (A.1) in integral form

$$\mathbf{h}(t+\Delta t) - \mathbf{h}(t) = \int_t^{t+\Delta t}\left[\mathbf{F}(\mathbf{h}(t')) + \sum_{\ell=1}^{\infty}\mathbf{G}^{\ell}(\mathbf{h}(t'))\cdot\boldsymbol{\mathcal{S}}^{\ell}(t')\right]dt' \tag{A.5}$$

and get the change of $\mathbf{h}$ in a small but finite time interval needed to calculate the expansion coefficients from Eq. (A.4). We expand $\mathbf{F}$ and $\mathbf{G}^{\ell}$ in the integrand around $\mathbf{h}(t)$, namely the value at the beginning of the integration interval

$$\mathbf{F}(\mathbf{h}(t')) = \mathbf{F}(\mathbf{h}(t)) + \sum_i \frac{\partial \mathbf{F}(\mathbf{h}(t))}{\partial h_i}\left[h_i(t') - h_i(t)\right] + \ldots \tag{A.6}$$

$$\mathbf{G}^{\ell}(\mathbf{h}(t')) = \mathbf{G}^{\ell}(\mathbf{h}(t)) + \sum_i \frac{\partial \mathbf{G}^{\ell}(\mathbf{h}(t))}{\partial h_i}\left[h_i(t') - h_i(t)\right] + \ldots. \tag{A.7}$$

The ellipses stand for terms of higher order in $h_i(t') - h_i(t)$. This we insert in the integral form Eq. (A.5) and get

$$\begin{aligned}\mathbf{h}(t+\Delta t) - \mathbf{h}(t) = &\int_t^{t+\Delta t} \left[ \mathbf{F}(\mathbf{h}(t)) + \sum_{\ell=1}^{\infty} \mathbf{G}^{\ell}(\mathbf{h}(t)) \cdot \boldsymbol{\mathcal{S}}^{\ell}(t') \right] dt' \\ &+ \int_t^{t+\Delta t} \sum_i \left[ \frac{\partial \mathbf{F}(\mathbf{h}(t))}{\partial h_i} + \sum_{\ell=1}^{\infty} \frac{\partial \mathbf{G}^{\ell}(\mathbf{h}(t))}{\partial h_i} \cdot \boldsymbol{\mathcal{S}}^{\ell}(t') \right] \\ &\times \left[ h_i(t') - h_i(t) \right] dt' + \ldots . \end{aligned} \tag{A.8}$$

We can expand $h_i(t') - h_i(t)$ in the second term using Eq. (A.8) again and get

$$\begin{aligned}\mathbf{h}(t+\Delta t) - \mathbf{h}(t) \approx &\int_t^{t+\Delta t} \left[ \mathbf{F}(\mathbf{h}(t)) + \sum_{\ell=1}^{\infty} \mathbf{G}^{\ell}(\mathbf{h}(t)) \cdot \boldsymbol{\mathcal{S}}^{\ell}(t') \right] dt' \\ &+ \int_t^{t+\Delta t} \sum_i \left\{ \left[ \frac{\partial \mathbf{F}(\mathbf{h}(t))}{\partial h_i} + \sum_{\ell=1}^{\infty} \frac{\partial \mathbf{G}^{\ell}(\mathbf{h}(t))}{\partial h_i} \cdot \boldsymbol{\mathcal{S}}^{\ell}(t') \right] \right. \\ &\left. \times \int_t^{t'} \left[ F_i(\mathbf{h}(t)) + \sum_j \sum_{m=1}^{\infty} G_{ij}^{m}(\mathbf{h}(t)) \mathcal{S}_j^{m}(t'') \right] dt'' \right\} dt' + \ldots . \end{aligned} \tag{A.9}$$

Iterating these substitutions finally yields an infinite sum of terms only depending on $\mathbf{h}(t)$, *i.e.*, only the value of $h$ at the beginning of the integration interval. In order to calculate the first Kramers–Moyal expansion coefficient we need to take the average of Eq. (A.9). Since $\langle \boldsymbol{\mathcal{S}}^{\ell}(t) \rangle = 0$ we are left with

$$\begin{aligned}\langle h_i(t+\Delta t) - h_i(t) \rangle = &F_i(\mathbf{h}(t))\, \Delta t + \sum_{j,k,k'} \sum_{\ell,m=1}^{\infty} \frac{\partial G_{ik'}^{\ell}(\mathbf{h}(t))}{\partial h_k} \\ &\times G_{kj}^{m}(\mathbf{h}(t)) \left\langle \int_t^{t+\Delta t} \int_t^{t'} \mathcal{S}_{k'}^{\ell}(t')\, \mathcal{S}_j^{m}(t'')\, dt'' dt' \right\rangle + \ldots . \end{aligned} \tag{A.10}$$

The remaining terms are higher order in $\Delta t$. Each term on the right-hand side of Eq. (A.9) is under at least one integral. The order of terms without noise is therefore given by the number of integrals. Terms containing an odd number of noises are zero and terms containing an even number of noises, say $p$, have at

least $p$ integrals. Each pair of noises gives a delta function in time and therefore reduces the order of the term by $p/2$. We only need terms up to linear order in $\Delta t$ and therefore only terms containing at most two integrals have to be considered. According to the rules of Ito calculus, the average in the second term is zero and we get for the first Kramers–Moyal expansion coefficient

$$\mathbf{D}^{(1)}(\mathbf{h}(t)) = \lim_{\Delta t \to 0} \frac{\langle \mathbf{h}(t+\Delta t) - \mathbf{h}(t) \rangle}{\Delta t} = \mathbf{F}(\mathbf{h}(t)). \tag{A.11}$$

Next we calculate the second Kramers–Moyal coefficient. We use Eq. (A.9) and $\langle \boldsymbol{\mathcal{S}}^{\ell}(t) \rangle = 0$ in order to calculate the average in Eq. (A.4)

$$\begin{aligned} &\left\langle [h_i(t+\Delta t) - h_i(t)] \left[ h_j(t+\Delta t) - h_j(t) \right] \right\rangle \\ &\quad = \sum_{k,k'} \sum_{\ell,m=1}^{\infty} G^{\ell}_{ik}(\mathbf{h}(t))\, G^{m}_{jk'}(\mathbf{h}(t)) \left\langle \int_t^{t+\Delta t} \mathcal{S}^{\ell}_k(t')\, dt' \int_t^{t+\Delta t} \mathcal{S}^{m}_{k'}(t'')\, dt'' \right\rangle + \ldots . \end{aligned} \tag{A.12}$$

All other terms are either zero or of higher than first order in $\Delta t$, see the paragraph after Eq. (A.10). In the limit $\Delta t \to 0$ we get with Eq. (A.2)

$$\begin{aligned} D^{(2)}_{ij}(\mathbf{h}(t)) &= \lim_{\Delta t \to 0} \frac{\left\langle [h_i(t+\Delta t) - h_i(t)] \left[ h_j(t+\Delta t) - h_j(t) \right] \right\rangle}{2\,\Delta t} \\ &= T \sum_{k} \sum_{\ell=1}^{\infty} G^{\ell}_{ik}(\mathbf{h}(t))\, G^{\ell}_{jk}(\mathbf{h}(t)). \end{aligned} \tag{A.13}$$

Using Eq. (A.9) in the definition for higher Kramers–Moyal coefficients, namely Eq. (A.4) for $n > 2$, the only terms which are left after taking the average are of order $\Delta t^2$ or higher. Therefore all higher Kramers–Moyal coefficients are zero, see also the corresponding argument for the Kramers–Moyal coefficients for a Langevin equation with only one variable in.[20] (Sec. 3.3.2) The Kramers–Moyal expansion in Eq. (A.3) therefore collapses to the Fokker–Planck equation

$$\frac{\partial \mathcal{W}(\mathbf{h}, t)}{\partial t} = -\sum_i \frac{\partial}{\partial h_i} \left\{ F_i(\mathbf{h}) - T \sum_{j,k} \frac{\partial}{\partial h_j} \left[ \sum_{\ell=1}^{\infty} G^{\ell}_{ik}(\mathbf{h})\, G^{\ell}_{jk}(\mathbf{h})\, \mathcal{W}(\mathbf{h}, t) \right] \right\}. \tag{A.14}$$

Following the same calculations as presented above, we can immediately see that the Kramers–Moyal coefficients for the Langevin equation with only one noise term per dependent variable $h_i$

$$\frac{\partial \mathbf{h}}{\partial t} = \mathbf{F}(\mathbf{h}) + \mathbf{G}(\mathbf{h}) \cdot \boldsymbol{\mathcal{N}}(t), \tag{A.15}$$

with

$$\langle \boldsymbol{\mathcal{N}}(t) \rangle = 0 \quad \text{and} \quad \langle \mathcal{N}_i(t)\, \mathcal{N}_j(t') \rangle = 2\, T\, \delta_{ij}\, \delta(t - t') \tag{A.16}$$

are

$$\mathbf{D}^{(1)}(\mathbf{h}(t)) = \mathbf{F}(\mathbf{h}(t)) \tag{A.17}$$

and

$$D^{(2)}_{ij}(\mathbf{h}(t)) = T \sum_k G_{ik}(\mathbf{h}(t))\, G_{jk}(\mathbf{h}(t)). \tag{A.18}$$

The Fokker–Planck equation is therefore given by

$$\frac{\partial \mathcal{W}(\mathbf{h}, t)}{\partial t} = -\sum_i \frac{\partial}{\partial h_i} \left\{ F_i(\mathbf{h}) - T \sum_{j,k} \frac{\partial}{\partial h_j} \left[ G_{ik}(\mathbf{h})\, G_{jk}(\mathbf{h})\, \mathcal{W}(\mathbf{h}, t) \right] \right\}. \tag{A.19}$$

The two Langevin Eqs. (A.1) and (A.15) are equal if the probability densities $\mathcal{W}(\mathbf{h}, t)$ are equal at any time for equal initial conditions. This means that the Fokker–Planck equations have to be equal. These are equal if the Kramers–Moyal coefficients are equal. The first coefficients are equal because the deterministic parts of Eqs. (A.1) and (A.15) are equal. Therefore we get a condition on $\mathbf{G}^{\ell}(\mathbf{h})$ and $\mathbf{G}(\mathbf{h})$ if we want equality of the second coefficients in Eqs. (A.13) and (A.18), respectively.

## APPENDIX B. DISCRETIZATION OF THE FOURTH-ORDER DIFFERENTIAL OPERATOR

Let us briefly describe the discretisation of the deterministic thin-film equation (i.e., Eq. (19) for $\tau = 0$)

$$\frac{\partial h}{\partial t} = \partial_x \left[ M(h)\, \partial_x p \right] \tag{B.1a}$$

$$p = -\nabla_x^2 h + \Phi'(h). \tag{B.1b}$$

Introducing for a small cut-off $0 < \sigma \ll 1$ the shifted mobility

$$m_\sigma(h) := \begin{cases} \frac{1}{3}\, h^3 & \text{for} \quad h \geq \sigma \\ \frac{1}{3}\, \sigma^3 & \text{else,} \end{cases} \tag{B.2}$$

we define the discrete mobility $M_\sigma$ for the finite element approximation $H \in V_{per}^N$ in the subinterval $E_i := (x_i, x_{i+1})$, $i = 0, \ldots, N-1$, by the formula

$$M_\sigma(H)|_{E_i} := \begin{cases} m_\sigma(\bar{H}_i) & \text{if} \quad \bar{H}_i = \bar{H}_{i+1} \\ (\bar{H}_{i+1} - \bar{H}_i) \left( \int_{\bar{H}_i}^{\bar{H}_{i+1}} \frac{1}{m_\sigma(s)}\, ds \right)^{-1} & \text{if} \quad \bar{H}_i \neq \bar{H}_{i+1}. \end{cases} \tag{B.3}$$

Observe that the degeneracy of the equation is mimicked by the fact that $M_\sigma(H)|_{E_i}$ becomes small if $\bar{H}_i$ or $\bar{H}_{i+1}$ tend to zero. The $\sigma$-truncation in Eq. (B.2) is used to guarantee wellposedness of Eq. (B.3). In particular, the special choice of $M_\sigma$ guarantees that all the integral estimates from the continuous setting carry over to the discrete setting. Therefore, non-negativity of discrete solutions can be proven in a natural way, see[2] for more details.

Decomposing $\Phi$ into a sum $\Phi = \Phi_+ + \Phi_-$ with $\Phi_+$ non-negative and convex and $\Phi_-$ concave, the following scheme was suggested in.[32] For given $H^0 \in V_{per}^N$ and $n \in \mathbb{N}$, find iteratively functions $H^{n+1}$ and $P^{n+1}$ in $V_{per}^N$ such that

$$(H^{n+1} - H^n, \Theta)_N + \tau_n (M_\sigma(H^{n+1}) \nabla P^{n+1}, \nabla \Theta) = 0 \tag{B.4a}$$

$$(\nabla H^{n+1}, \nabla \Psi) + (\Phi'_+(H^{n+1}), \Psi)_N + (\Phi'_-(H^n), \Psi)_N = (P^{n+1}, \Psi)_N \tag{B.4b}$$

for all test functions $\Theta, \Psi \in V_{per}^N$. Here, $\tau_n = t_{n+1} - t_n$ is the time-increment. Introducing the mobility weighted stiffness matrix $(L_N^M(\bar{H}))_{ij} := \int_I M_\sigma(\bar{H}) \nabla \phi_i \nabla \phi_j$, the system (B.4) is written equivalently in matrix form as follows. For given $\bar{H}^n \in \mathbb{R}^N$, find $\bar{H}^{n+1} \in \mathbb{R}^N$ such that

$$\begin{aligned} \bar{H}^{n+1} - \bar{H}^n + \tau_n M_N^{-1} \cdot L_N^M(\bar{H}^{n+1}) \cdot \big[ & M_N^{-1} \cdot L_N \cdot \bar{H}^{n+1} \\ & + \Phi'_+(\bar{H}^{n+1}) + \Phi'_-(\bar{H}^n) \big] = 0. \end{aligned} \tag{B.5}$$

Note that $M_N^{-1} L_N^M(\bar{H}^{n+1}) M_N^{-1} L_N$ is a sparse matrix since the lumped masses matrix $M_N$ is diagonal. For the uniform discretization used here the diagonal elements of $M_N$ are $a$ and we can replace $M_N^{-1}$ in Eq. (B.5) by $\frac{1}{a}$. With $\Phi'_\pm(\bar{H})$ we denote the component vector of $\Phi'_\pm(H)$.

## APPENDIX C. ITO VS. STRATONOVICH CALCULUS

In Appendix A we calculate the Kramers–Moyal expansion coefficients in Ito calculus. In this section we will show, that for the stochastic thin film Eqs. (17) and (19) Ito and Stratonivich calculus are equivalent by showing that the spurious drift term in the first Kramers–Moyal expansion coefficients vanishes.

The only point in Appendix A where the difference between Ito and Stratonovich calculus becomes important is the evaluation of the stochastic integrals in the second term on the right hand side of Eq. (A.10). The result for Stratonovich calculus can be obtained by assuming that the $\delta$-function in Eq. (A.2)

is symmetric with respect to the argument and we get for the first Kramers–Moyal expansion coefficient

$$\mathbf{D}^{(1)}(\mathbf{h}(t)) = \mathbf{F}(\mathbf{h}(t)) + T \sum_{k,k'} \sum_{\ell=1}^{\infty} \frac{\partial G^{\ell}_{ik'}(\mathbf{h}(t))}{\partial h_k(t)} G^{\ell}_{kk'}(\mathbf{h}(t)). \tag{C.1}$$

The difference to the first Kramers–Moyal expansion coefficient in Ito calculus in Eq. (A.11) is the second term on the right hand side, the so-called spurious drift term. We get with $G^{\ell}_{ij}(\mathbf{h}) = \nabla^{s}_{ij}\, q^{\ell}(h_j)$ for the spurious drift term for Eq. (32)

$$T \sum_{k,k'} \sum_{\ell=1}^{\infty} \nabla^{s}_{ik'} \frac{\partial q^{\ell}(h_{k'})}{\partial h_k} \nabla^{s}_{kk'}\, q^{\ell}(h_{k'}) = 0. \tag{C.2}$$

The reason is, that $\frac{\partial q^{\ell}(h_{k'})}{\partial h_k} = \delta_{kk'} \frac{\partial q^{\ell}(h_k)}{\partial h_k}$ is symmetric in $k$ and $k'$, while the symmetric finite difference operator $\nabla^{s}_{kk'}$ is antisymmetric in $k$ and $k'$. With the same argument the spurious drift term for Eq. (33) vanishes.

Since the only difference between Ito and Stratonovich calculus is the spurious drift term, the Fokker–Planck equation for Eqs. (32) and (33) are equal and therefore independent of the calculus used.

## ACKNOWLEDGMENT

The numerical simulations for the stochastic thin-film equation have been performed by Cand.math. Fabian Klingbeil who has been supported by grant Gr1693-1/2 of Deutsche Forschungsgemeinschaft.

*Note added:* The same stochastic thin-film Eq. (70) was derived independently in a recent study of droplet spreading.[33]

## REFERENCES

1. A. Oron, S. H. Davis and S. G. Bankoff, Long-scale evolution of thin liquid films. *Rev. Mod. Phys.* **69**:931 (1997).
2. G. Grün and M. Rumpf, Nonnegativity preserving convergent schemes for the thin film equation. *Numer. Math.* **87**:113 (2000).
3. G. Grün, On the convergence of entropy consistent for lubrication-type equations in multiple space dimensions. *Math. Comp.* **72**:1251 (2003).
4. K. R. Mecke, Integral geometry in statistical physics. *Int. J. Mod. Phys. B* **12**: 861 (1998).
5. J. Becker, G. Grün, R. Seemann, H. Mantz, K. Jacobs, K. R. Mecke and R. Blossey, Complex dewetting scenarios captured by thin film models. *Nature Materials* **2**: 59 (2003).
6. R. Konrad, Master's thesis, Universität Ulm (2003).
7. L. D. Landau and E. M. Lifšic, *Hydrodynamik*, vol. VI of *Lehrbuch der Theoretischen Physik* 5th ed. (Akademie Verlag, 1991).
8. K. T. Mashiyama and H. Mori, Origin of the Landau-Lifshitz hydrodynamic fluctuations in nonequilibrium systems and a new method for reducing the Boltzmann equation. *J. Stat. Phys.* **18**:385 (1978).

9. D. Forster, D. R. Nelson and M. J. Stephen, Long-time tails and the large-eddy behavior of a randomly stirred fluid. *Phys. Rev. Lett.* **36**:867 (1976).
10. D. Forster, D. R. Nelson and M. J. Stephen, Large-distance and long-time properties of a randomly stirred fluid. *Phys. Rev. A* **16**:732 (1977).
11. P. C. Hohenberg and J. B. Swift, Effects of additive noise at the onset of Rayleigh-Bénard convection. *Phys. Rev. A* **46**:4773 (1992).
12. J. B. Swift, K. L. Babcock and P. C. Hohenberg, Effects of thermal noise in Taylor-Couette flow with corotation and axial through flow. *Physica A* **204**:625 (1994).
13. M. Moseler and U. Landman, Formation, stability, and breakup of nanojets. *Science* **289**:1165 (2000).
14. D. G. A. L. Aarts, M. Schmidt and H. N. W. Lekkerkerker, Direct visual observation of thermal capillary waves. *Science* **304**:847 (2004).
15. S. Dietrich and M. Napiórkowski, Microscopic derivation of the effective interface Hamiltonian for liquid-vapor interfaces. *Physica A* **177**:437 (1991).
16. D. Blömker, S. Maier-Paape and T. Wanner, Spinodal decomposition for the Cahn-Hilliard-Cook equation. *Comm. Math. Phys.* **223**:553 (2001).
17. D. Blömker, S. Maier-Paape and T. Wanner, Phase separation in stochastic Cahn-Hillard models. *Preprint, RWTH Aachen* (2004).
18. C. Cardon-Weber, Cahn-Hilliard stochastic equation: existence of the solution and of its density. *Bernoulli* **7**:777 (2001).
19. G. Da Prato and A. Debussche, Stochastic Cahn-Hilliard equation. *Nonlinear Anal. TMA* **26**:241 (1995).
20. H. Risken, *The Fokker-Planck Equation*, vol. 18 of *Springer Series in Synergetics* (Springer, Berlin, 1984).
21. C. W. Gardiner, *Handbook of Stochastic Methods*, vol. 13 of *Springer Series in Synergetics* (Springer, Berlin, 1983).
22. F. Bernis and A. Friedman, Higher order nonlinear degenerate parabolic equations. *J. Differential Equations* **83**:179–206 (1990).
23. A. Bertozzi and M. Pugh, The lubrication approximation for thin viscous films: regularity and long time behaviour of weak solutions. *Comm. Pure Appl. Math.* **49**:85–123 (1996).
24. E. Beretta, M. Bertsch and R. Dal Passo, Nonnegative solutions of a fourth order nonlinear degenerate parabolic equation. *Arch. Ration. Mech. Anal.* **129**:175–200 (1995).
25. G. Grün, Droplet spreading under weak slippage: existence for the Cauchy problem. *Comm. Partial Diff. Equations* **29**:1697–1744 (2004).
26. A. de Bouard, A. Debussche and Y. Tsutsumi, White noise driven Kortweg-de Vries equations. *J. Funct. Anal.* **169**:532 (1999).
27. G. Tessitore and J. Zabczyk, Strict positivity for stochastic heat equations. *Stochastic Processes Appl.* **77**:83 (1998).
28. J. Towers, Convergence of a difference scheme for conservation laws with a discontinuous flux. *SIAM J. Num. Anal.* **38**:681 (2000).
29. A. Bertozzi, G. Grün and T. Witelski, Dewetting films: bifurcations and concentrations. *Nonlinearity* **14**:1569 (2001).
30. N. Dirr and G. Grün, On the stochastic thin-film equation – an existence result, *in preparation*.
31. K. R. Mecke, R. Fetzer and M. Rauscher (2005), to be published.
32. G. Grün and M. Rumpf, Simulation of singularities and instabilities arising in thin film flow. *Eur. J. Appl. Math.* **12**:293 (2001).
33. B. Davidovitch, E. Moro and H.A. Stone, Spreading of viscous fluid drops on a solid substrate assistd by thermal fluctuations. *Phys. Rev. Lett.* **95**:244505 (2005).